INSTITUTE OF PHYSICS PUBLISHING PHYSICS IN MEDICINE AND BIOLOGY

Phys. Med. Biol. **47** (2002) R85–R106 PII: S0031-9155(02)21840-0

TOPICAL REVIEW

Inorganic scintillators in medical imaging

Carel W E van Eijk

Delft University of Technology, IRI, Radiation Technology, Mekelweg 15, 2629 JB Delft, The Netherlands

E-mail: vaneijk@iri.tudelft.nl

Received 4 January 2002
Published 5 April 2002
Online at stacks.iop.org/PMB/47/R85

Abstract
A review of medical diagnostic imaging methods utilizing x-rays or gamma rays and the application and development of inorganic scintillators is presented.

1. Introduction

Inorganic scintillators are employed in most of the current medical diagnostic imaging modalities using x-rays or gamma rays (see e.g. Webb (1990)). This is explained by the comparatively good detection efficiency of inorganic scintillators for hard radiation. Yet, the various diagnostic methods differ considerably and consequently the radiation detector requirements also differ. These requirements are not always met by the scintillator specifications. This is one of the reasons for continuous scintillator R&D. The other reasons are the need for (1) new, digital diagnostic systems with an excellent image quality and a short image acquisition time and (2) excellent quality real-time imaging systems for interventional radiology at a low radiation dose. After a discussion of the various diagnostic methods in which the emphasis is put on the expanding field of positron emission tomography, a review of the specifications of the employed scintillators and some recent scintillator research is presented.

2. X-ray imaging

In x-ray radiography (*static* imaging) an attenuation profile of a part of the human body is projected onto a two-dimensional position-sensitive radiation detector (PSD) using the focus of an x-ray tube as a point source. Thus, information on anatomical detail is obtained. The method is applied in almost all fields of clinical practice. A variety of radiation detectors are used. For example, at present, for chest radiography x-ray phosphor-screen-film cassettes and storage-phosphor plates (computed radiography), both typically of 35×43 cm^2, are applied as the PSD on a large scale (Webb 1990). In most cases Gd_2O_2S:Tb is used as the x-ray intensifying screen phosphor, i.e. the scintillator (Blasse and Grabmaier 1994).

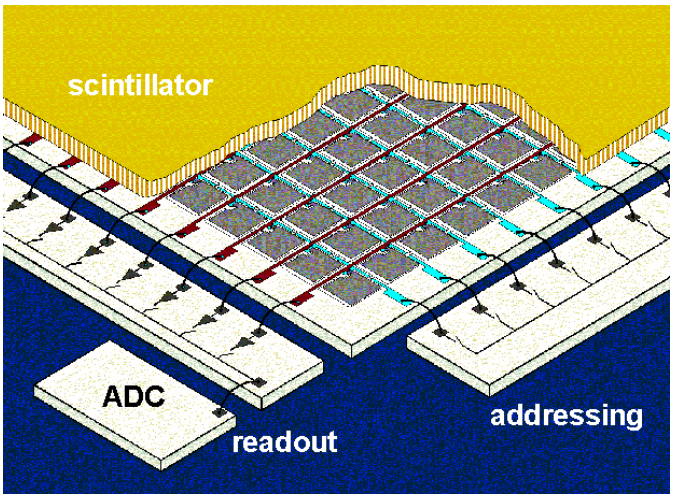

Figure 1. Schematic of a flat-panel detector. An array of amorphous-silicon diodes positioned on a glass plate is covered by a scintillator screen of columnar grown CsI:Tl. Addressing lines and read-out lines are respectively coming from and going to chips at the edge of the plate (courtesy Philips Research Laboratories, Aachen).

The standard storage-phosphor material is $BaFBr_{1-x}I_x$:Eu ($x \leqslant 0.2$) (Fuji, Agfa, Eastman Kodak[1]) (Sonoda *et al* 1983). Furthermore, a digital chest-radiography system is used based on the electrostatic read-out of a drum covered with an amorphous-selenium (a-Se) semiconductor layer as the PSD (Thoravision, Philips) (Webb 1990, Neitzel *et al* 1994). Recently, new digital radiography (DR) systems have been introduced; for example, Eastman Kodak developed a system employing an a-Se photoconductor layer deposited on top of an amorphous-silicon (a-Si:H) thin-film transistor array (Direct View). For the principle of detector operation, see Soltani *et al* (1999). The active image area is 35×43 cm^2, the pixel pitch is 139 μm. Agfa introduced a system employing a Gd_2O_2S:Tb phosphor screen deposited on top of an array of a-Si:H photodiodes coupled to an array of thin-film transistors, active area 43×43 cm^2, pixel size 160×160 μm^2 (DR-Thorax).

A PSD such as the a-Se/a-Si:H system, which converts x-rays into electrons, is called *direct*, as opposed to a PSD that makes use of the conversion of x-rays into light and subsequently of light into electrons, such as the Gd_2O_2S:Tb/a-Si:H system, which is called *indirect*. It appears that indirect flat-panel PSDs analogous to that of Agfa but employing a CsI:Tl scintillator screen will find large scale application in the very near future. Canon, General Electric, Varian and TRIXELL (a joint venture of Philips, Siemens and Thomson) are following this path. TRIXELL is developing a 43×43 cm^2 flat-panel PSD with a pixel pitch of 143 μm (Pixium 4600). For the principle of operation, see figure 1 (Jing *et al* 1994, Schiebel *et al* 1994) and also Moy (1999).

In mammography film-screen cassettes of 18×24 cm^2 are generally used. In this case a resolution of 0.1 mm is required to observe microcalcifications. Conventional film-screen systems usually consist of two equal phosphor-binder layers (thickness up to $\sim$0.3 mm per layer) and two equal emulsion layers, one on each side of the film base. More advanced systems for chest radiography are asymmetric in structure, i.e. the two screens have different layer thicknesses and the two emulsions are of different contrast (InSight, Eastman Kodak)

[1] For company-related information the reader is referred to company websites.

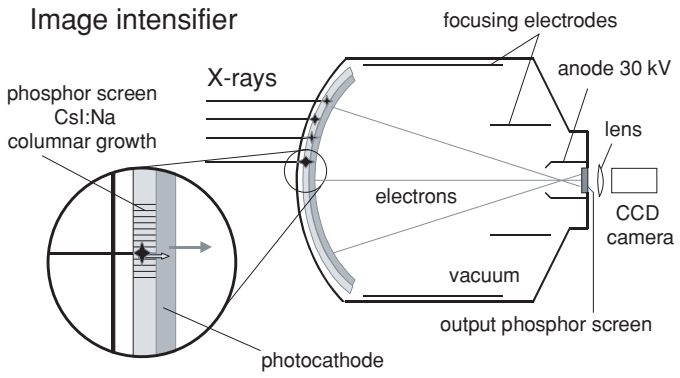

Figure 2. Schematic of an image intensifier system.

(Gray *et al* 1993). In mammography only one relatively thin screen (∼0.07 mm) and one emulsion are used to realize the required resolution. As for efficiency, it should be noted that relatively low-energy x-rays, e.g. produced at a tube voltage of 28 kV in a molybdenum anode and filtered by 0.03 mm magnesium, are used for mammography compared to higher energy x-rays, for example, produced at a tube voltage of 150 kV in a tungsten anode and filtered by several millimetres of aluminium and also often by a few tenths of millimetres of copper, for chest radiography. Fischer Imaging Corporation and TREX Medical have introduced DR systems based on a phosphor screen coupled to charge-coupled devices (CCDs) by means of fibre optical reducers. General Electric developed a digital mammography system based on the CsI:Tl a-Si:H concept, 19 × 23 cm^2, pixel size 100 × 100 μm^2 (Senographe 2000D) (Muller 1999).

In dentistry, where very small detectors of ∼2 × 3 cm^2 to 3 × 4 cm^2 are used for intra-oral radiography (∼65 kVp x-rays), direct radiation detection in a CCD is applied, in addition to the traditional intra-oral film-package and the storage-phosphor plate (van der Stelt 2001). Pixel pitches are in the range 20–40 μm. Similar methods are applied for panoramic and cephalometric radiography.

For fluoroscopy (*dynamic* imaging) a system is needed which responds fast enough to provide *real-time* images of motion in the region of interest of the human body. At present the x-ray image-intensifier-based system is the workhorse (Webb 1990, Hell *et al* 2000). A CsI:Na scintillator screen on the inside of the entrance window absorbs the x-rays; see figure 2. Scintillation photons are converted into electrons by means of a photocathode (e.g. Cs_3Sb). The electrons are accelerated and projected onto an output phosphor (e.g. ZnS:Cu, (Zn, Cd)S:Cu, (Zn, Cd)S:Ag), resulting in an intermediate, reduced image. In the early days the light thus produced was observed by means of a TV camera. Today the intermediate image is observed by means of advanced CCD systems. Depending on the application, image intensifier screen diameters are used in the range 23–40 cm, providing 1 k × 1 k pixel images, at frame rates up to 30 frames per second.

Image-intensifier-based systems are also widely used for radiographic imaging and for simulation in radiation therapy planning (radiographic and fluoroscopic) (Williams and Thwaites 2000).

The image intensifier systems are very bulky and research to replace these detectors by much more practicable devices is in progress. Most interesting is the development of large ∼40 × 40 cm^2 fluoroscopic systems based on the CsI:Tl/a-Si:H flat-panel concept.

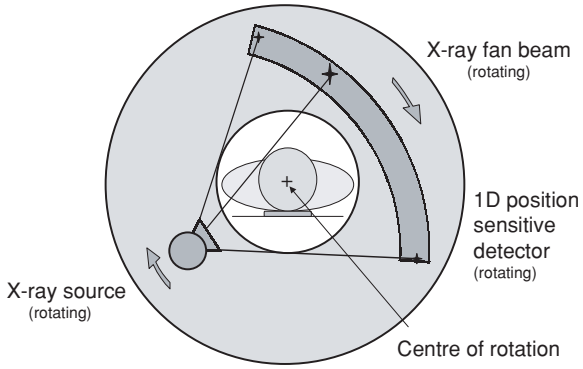

Figure 3. Schematic of an x-ray CT system.

Summarizing, we note that, apart from the a-Se-semiconductor-based PSDs and the dental CCDs, all systems are luminescence based. The screen phosphor Gd_2O_2S:Tb, scintillators CsI:Na and Cs:Tl, and storage-phosphor $BaFBr_{1-x}I_x$:Eu are dominating the x-ray imaging field. We will return to these devices in section 6.

3. X-ray computed tomography

In principle, in x-ray computed tomography (CT) the body is consecutively irradiated from a large number of directions by an x-ray fan beam (Kalender 2000); see figure 3. Attenuation profiles are registered and from them cross-sectional images of the body are reconstructed. Actually, sophisticated scan modes are used such as multi-slice spiral CT combined with volume reconstruction. Applications are found in many fields of clinical practice.

To measure the profiles, a segment of a circle, radius ∼1 m, centre on the x-ray source, is covered with up to ∼1000 small detectors which form a one-dimensional PSD. The segment rotates with the x-ray source (tube) for detecting the fan beam at all angular settings (figure 3). X-ray energies are in the range up to ∼140 keV (80–140 kVp) and consequently an inorganic scintillator is the obvious detection medium. $CdWO_4$, $Bi_4Ge_3O_{12}$ (BGO) and CsI:Tl, read out by photodiodes (integrating mode), have been used in the past. However, for various reasons these scintillators are less favourable; for example, light yields are low or/and matching with the quantum efficiency curve of the light detecting diodes is poor ($CdWO_4$, BGO). Furthermore, at each angular position a certain amount of light is accepted due to the slow scintillation response on radiation absorbed at the previous angular position (primary decay and afterglow). In a modern CT system the rotation time is typically <1 s. A preferred condition is, for example, that <0.01% of the maximum scintillation intensity is emitted after ∼3 ms (Blasse and Grabmaier 1994, Hupke and Doubrava 1999). The afterglow of CsI:Tl is clearly too high (table 1). Another undesirable effect is radiation damage, resulting in a change of light output, e.g., an increase in CsI:Tl and a decrease in $CdWO_4$. Furthermore, $CdWO_4$ is preferably avoided because of its toxicity.

One way to remedy the shortcomings has been to employ pressurized Xe gas ionization detectors; for example, in one of the Siemens SOMATOM systems we encounter an arc of 768 xenon sensors of 1.2×18 mm^2 and a depth of several centimetres. However, the detection efficiency is not high enough.

A very interesting development was the preparation of scintillators using advanced ceramic technologies, and the introduction of co-doping to reduce the afterglow (Grabmaier and Rossner 1993, Blasse and Grabmaier 1994, Greskovich and Duclos 1997). Examples are

Table 1. Inorganic scintillators for medical imaging (for references see text).

	Density (g cm^{-3})	ρZ^4_{eff} (10^6)	Attenuation length at 511 keV (mm)/ prob. phot. eff. (%)	Hygro-scopicity	Light yield (photons/ MeV)	Decay time (ns)	Afterglow (% after 3 ms/100 ms)	Emission maximum (nm)	$\Delta E/E$ (FWHM) at 662 keV (%) PMT read-out	Δt (ps) /BaF_2 /^{60}Co
CsI:Na	4.51	38	22.9/21	Yes	40 000	630		420	7.4	
CsI:Tl	4.51	38	22.9/21	Slightly	66 000	800–>6×10^3	>2/0.3	550	6.6 (PMT)/ 4.3 (SDD)[a]	
$CaWO_4$	6.1	89	13.6/32	No	20 000[b]			420	Integrating mode	
$YTaO_4$:Nb	7.5	96	11.8/29	No	40 000[b]			410	Integrating mode	
Gd_2O_2S:Tb	7.3	103	12.7/27	No	60 000[b]	1×10^6		545	Integrating mode	
Gd_2O_2S:Pr,Ce,F	7.3	103	12.7/27	No	35 000[b]	4×10^3	<0.1/<0.01	510	Integrating mode	
Gd_2O_2S:Pr (UFC)	7.3	103	12.7/27	No	50 000[b]	3×10^3	0.02/0.002	510	Integrating mode	
$Y_{1.34}Gd_{0.60}O_3$:$(Eu,Pr)_{0.06}$[c] (Hilight)	5.9	44	17.8/16	No	42 000[b]	1×10^6	4.9/<0.01	610	Integrating mode	
$Gd_3Ga_5O_{12}$:Cr,Ce	7.1	58	14.8/18	No	40 000[b]	140×10^3	<0.1/0.01	730	Integrating mode	
$CdWO_4$	7.9	134	11.1/29	No	20 000[b]	5×10^3	<0.1/0.02	495	6.8	
Lu_2O_3:Eu,Tb	9.4	211	8.7/35	No	30 000[b]	$>10^6$	>1/0.3	611	Integrating mode	
$CaHfO_3$:Ce	7.5	139	11.6/30	No	~10 000[b]	40		390	Integrating mode	
$SrHfO_3$:Ce	7.7	122	11.5/28	No	~20 000[b]	40		390	Integrating mode	
$BaHfO_3$:Ce	8.4	142	10.6/30	No	~10 000[b]	25		400	Integrating mode	
NaI:Tl	3.67	24.5	29.1/17	Yes	41 000	230		410	5.6	
$LaCl_3$:Ce	3.86	23.2	27.8/14	Yes	46 000	25 (65%)		330	3.3	224
$LaBr_3$:Ce	5.3	25.6	21.3/13	Yes	61 000	35 (90%)		358	2.9	385
$Bi_4Ge_3O_{12}$ (BGO)	7.1	227	10.4/40	No	9 000	300		480	9.0	
Lu_2SiO_5:Ce (LSO)	7.4	143	11.4/32	No	26 000	40		420	7.9	
Gd_2SiO_5:Ce (GSO)	6.7	84	14.1/25	No	8 000	60		440	7.8	
$YAlO_3$:Ce (YAP)	5.5	7	21.3/4.2	No	21 000	30		350	4.3	
$LuAlO_3$:Ce (LuAP)	8.3	148	10.5/30	No	12 000	18		365	~15	
$Lu_2Si_2O_7$:Ce (LPS)	6.2	103	14.1/29	No	30 000	30		380	~10	

[a] Measured with a PMT and silicon drift detector (SDD).
[b] Measured at ~60–80 keV; all others at 662 keV.
[c] Proprietary co-dopant.

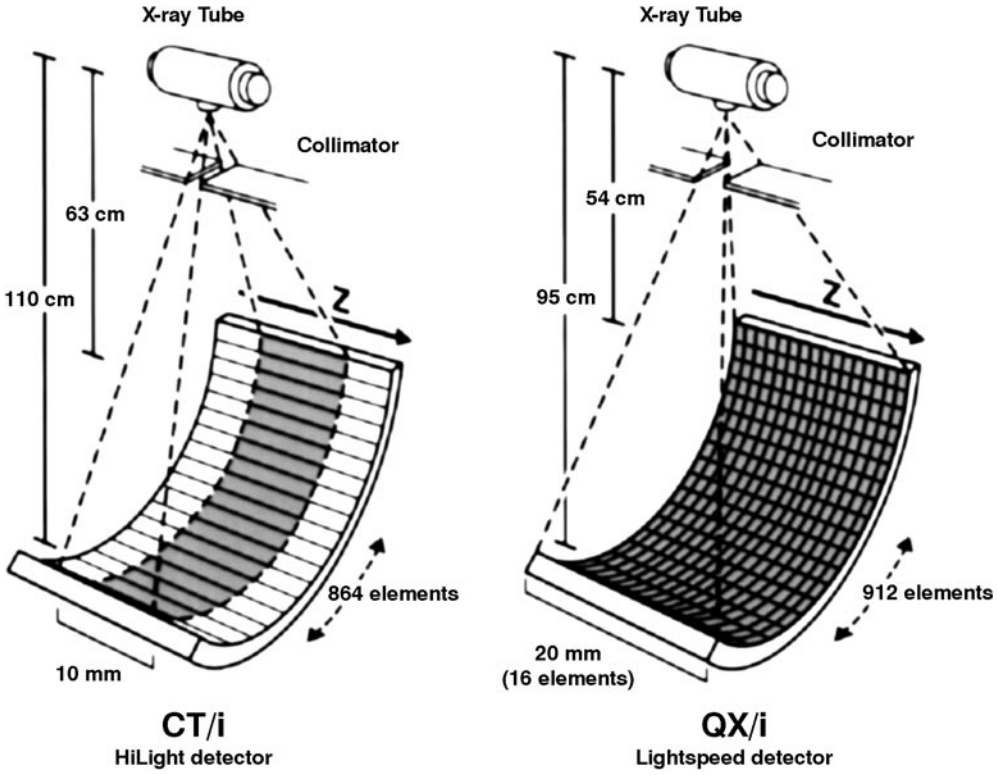

Figure 4. Schematics of GE curved x-ray CT detectors. One-dimensional PSD on the left, and two-dimensional array detector for multi-slice system on the right (from McCollough and Zink (1999), courtesy the authors and American Association of Physicists in Medicine).

$(Y,Gd)_2O_3:Eu^{3+}$ co-doped with Pr and Gd_2O_2S:Pr co-doped with Ce and F. In about 1998 several companies (General Electric, Marconi, Siemens, Toshiba) introduced two-dimensional array-detector arcs employing these types of ceramic scintillators; see figure 4. Thus multi-slice (spiral) imaging became possible (see e.g. McCollough and Zink (1999)). We will return to the ceramic scintillators in section 6.

4. Radionuclide imaging—single-photon emission

In radionuclide imaging based on single-photon emission, the gamma radiation emitted by a radiopharmaceutical introduced into the body is used either for simple projections (planar scintigraphy) or for single-photon emission computed tomography (SPECT) (Webb 1990). In both cases gamma cameras are used, originally typically circular with a diameter up to 50 cm, employing a monolithic NaI:Tl crystal plate (thickness ∼6–12 mm) and photomultiplier tube (PMT) read-out (e.g. hexagonal packing of 61 PMTs) (Short 1984, Jasczak *et al* 1980). Modern systems are square or rectangular, up to $\sim 50 \times 60$ cm^2, with the thickness of the NaI:Tl crystal plate up to 25 mm. In principle the photon-energy range is $\leqslant$400 keV. However, 140 keV from ^{99m}Tc labelled compounds is used most frequently. In scintigraphy large heavy collimator plates are used with parallel channels (diameter ∼2–3 mm) and 1:1 projection images of the distributions of the radiopharmaceuticals are obtained. In SPECT cone beam

Figure 5. Hybrid SPECT/PET system IRIX with three gamma cameras (courtesy Philips/Marconi Medical Systems).

collimation is used. Projections are measured from different sides of the body from which three-dimensional images are reconstructed.

The gamma camera operates in counting mode. For each event the distribution of the scintillation light over the PMTs is used to obtain the point of interaction. In general the information is extracted by means of a resistor network, connecting the PMTs (Anger logic). For SPECT (and PET, section 5) cameras with signal digitization per PMT are also used (e.g. ADAC/UGM). Recently Siemens/CTI introduced an experimental gamma camera for a hybrid SPECT/PET system, operating with arrays of small NaI:Tl and Lu_2SiO_5:Ce (LSO:Ce) crystals read out by PMTs (Jones *et al* 2001); see also the next section. In figure 5 an example of a hybrid SPECT/PET system with three gamma cameras operating in SPECT mode is shown.

5. Radionuclide imaging—positron emission tomography

5.1. Introduction

Positron emission tomography (PET) is a very powerful medical diagnostic method to observe the metabolism, blood flow, neurotransmission and handling of important biochemical entities (Webb 1990). PET is typically applied in neurology, oncology and cardiology. Imaging is realized by means of two 511 keV quanta which are emitted approximately collinearly when a positron, emitted by a radiopharmaceutical introduced into a patient, annihilates in tissue. The two annihilation quanta are detected position sensitively in coincidence (see figure 6). To a good approximation, the point of positron emission is situated on the line of response connecting the two detection positions. Many annihilations give many lines of

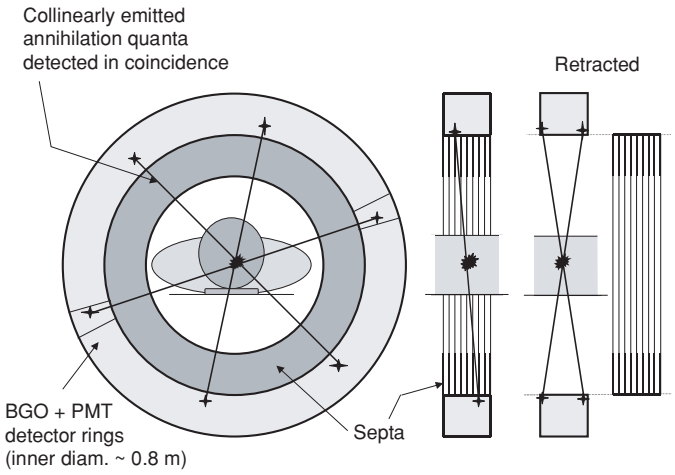

Figure 6. Schematic of PET system.

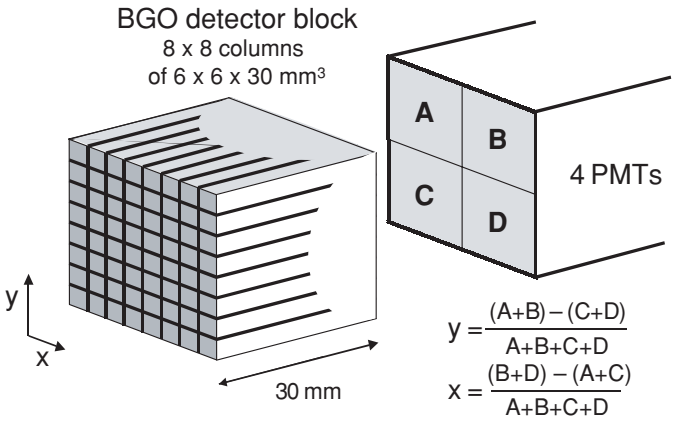

Figure 7. Schematic of BGO detector block showing saw cuts of 8 × 8 columns (left), to be coupled to four PMTs for position-sensitive light detection (right).

response (LOR) and in principle the three-dimensional reconstruction of the LOR represents the radiopharmaceutical distribution, i.e. the image.

For position-sensitive detection, a PET system consists, in general, of many rings with thousands of scintillation detectors (ECAT systems, Siemens/CTI) (see figures 6 and 7). BGO is the most used scintillator because of its good detection efficiency and large probability of photoelectric effect (40%) for 511 keV quanta (table 1). Yet, other PSD systems are also applied. ADAC/UGM employed six curved NaI:Tl crystals (2.54 cm thick) to form a cylinder, ∼25 cm high, ∼90 cm in diameter, read out by PMTs (CPET) (Adam *et al* 2001). NaI:Tl has the advantage that large, curved crystals can be produced relatively easy. Thus, acquisition over a large solid angle is realized. However, the intrinsic detection efficiency of NaI:Tl is significantly smaller than that of BGO (see table 1). Furthermore, we come across systems consisting of two gamma cameras (without collimator plates) facing each other (gamma camera PET, GC-PET). An example is the Millenium VG system of General Electric,

utilizing cameras with a 16 mm thick NaI:Tl crystal, a field of view of 54 × 40 cm^2, 59 PMTs and one ADC per PMT. Systems with 25 mm thick NaI:Tl crystals are also available.

There is much interest in introducing new scintillator materials. Other properties of BGO, such as its light yield, energy resolution and response time, make it less than optimal for application in PET. Siemens/CTI developed a new system based on LSO:Ce. In the ECAT Accel system, the BGO crystals used in the ECAT EXACT have been replaced by 25 mm LSO:Ce crystals (Townsend 2001). Furthermore, Siemens/CTI introduced the LSO:Ce-based high resolution research tomograph (HRRT) for brain studies (Wienhard *et al* 2001) and ADAC/UGM developed a brain PET system utilizing Gd_2SiO_5:Ce (GSO:Ce), the ALLEGRO (Karp *et al* 2001). In section 4 the hybrid SPECT/PET system based on NaI:Tl/LSO:Ce gamma cameras (Jones *et al* 2001) has been mentioned.

In addition to company-related R&D, many groups are actively developing new PET methods and techniques; as an example, we mention the use of liquid xenon (LXe) as a scintillator and ionization-chamber material (Chepel *et al* 1997, Collot *et al* 2000). Many papers on PET can be found in the proceedings of recent IEEE Nuclear Science Symposiums & Medical Imaging Conferences (NSS/MIC 1999, 2000).

For the sake of completeness it should be mentioned that various application-specific dedicated PET systems are being developed; for example, there is serious interest in application of PET in combination with mammography (positron emission mammography) (e.g. see Lecoq 2001). LSO:Ce is considered for utilization. Furthermore, animal studies can be performed for the development of radiopharmaceuticals for human use and for gene expression imaging and post-genomic investigations. Consequently, animal-PET systems are needed. Concorde introduced an LSO:Ce-based small-animal PET system (MicroPET). Several other small-animal PET systems have been developed (see e.g. Weber *et al* (2000) and Del Guerra *et al* (2000)). In both cases the relatively low density, small-Z scintillator $YAlO_3$:Ce (YAP:Ce) is employed.

It should be noted that multi-modality systems are becoming increasingly important. Combined CT–PET systems have been introduced by ADAC/Philips (Gemini), General Electric (Discovery series) and Siemens/CTI (Biograph) (Beyer *et al* 2000).

The properties of the PET scintillators are discussed in section 6. However, first PET-system requirements will be addressed somewhat more in detail.

5.2. PET-system requirements and sources of error

5.2.1. Detection efficiency. The detection efficiency for a 511 keV quantum (ε) is found squared in the coincidence efficiency. Consequently, it is very important to make ε as high as possible. This implies that both the solid angle subtended by the PET system and the intrinsic detector efficiency should be large. Only then can images be realized with a limited amount of radioactive material in a reasonable time. This explains why many detector rings are used and BGO is most often employed as the scintillator material.

In general BGO blocks with saw-cuts are applied (figure 7). Depending on the system these cuts provide 36 to 64 crystal columns of, e.g., 4 × 4, 3 × 6, 6 × 6 or 4 × 8 mm^2 cross sections, coupled at the base in such a way that the scintillation-light distribution allows the determination of the column hit by a radiation quantum using four PMTs or two PMTs with a dual structure, and Anger-type logic (Casey and Nutt 1986, DeGrado *et al* 1994, Wienhard *et al* 1994). Detector blocks are combined in rings to form typically 24–48 planes of scintillator columns. Using coincidences between scintillator columns in the same plane and cross-plane coincidences between columns in adjacent planes, image slices are obtained at a pitch of half the plane distance.

Originally, planes were separated by septa, i.e. lead collimator plates. In an actual PET scan a significant fraction (0.3–0.5) of the 511 keV quanta are Compton scattered in the patient. This gives a continuous background. The septa reduce this background significantly. With septa, cross-plane 511–511 keV coincidences are limited to differences of 3–4 planes (two-dimensional imaging). Modern systems can be operated with removed (retracted) septa where coincidences between many planes are accepted resulting in three-dimensional (3D) imaging (Townsend *et al* 1989, Cherry *et al* 1991). The CPET has no septa at all (Adam *et al* 2001). With septa retracted, the increased solid angle and consequently a higher 511–511 keV coincidence rate compensates to a certain extent for the increased Compton-scattering background. This background is reduced only by accepting events in the full-energy peak of the pulse-height spectrum (the better the resolution, the better the reduction will be; typical energy resolutions in PET systems are: for BGO 20% FWHM, for NaI:Tl ∼10% FWHM). However, many events with 511 keV quanta interacting in a scintillator due to the Compton effect will be eliminated as well. Consequently, depending on the PET system and specific application, one has to decide whether a full-energy peak window is used or a more relaxed window.

In a small-animal PET system the Compton scattering in a small animal plays a minor role. Consequently, Compton events in the pulse height spectrum are primarily due to scattering in the scintillator and can be accepted. Therefore, the threshold can be decreased. However, as a result position resolution may become worse as the Compton-scattered quantum may give a signal above threshold in a neighbouring crystal.

As for the scintillator one should realize that absorption by photoelectric effect per cm is proportional to ρZ^{3-4} with ρ the density and Z the effective atomic number. For 511 keV quanta the chance of photoelectric effect at $Z = 80$ is no more than 50%, the other 50% being the Compton effect (proportional to ρ). Depending on the kind of scintillator and crystal size, detection of both the Compton electron and the Compton-scattered photon in the same crystal may significantly contribute to the intensity of the full-energy peak.

5.2.2. Random coincidences and dead time. Random coincidences will occur, e.g. , if within the coincidence-time window one 511 keV quantum of each of the two pairs of annihilation quanta is detected and the other is emitted or Compton scattered by the patient in a direction outside the PET system. Random coincidences show up as a continuous background in an image. The ratio of true to random coincidences is inversely proportional to the coincidence-time resolution 2τ. The time resolution depends strongly on the response time of the scintillator, its light yield and light-detection efficiency. Using BGO, 2τ is in the order of 10 ns. A much smaller 2τ will reduce the background significantly. Furthermore, if 2τ is very small, time-of-flight information can be used to select a region of interest; for example, at $2\tau = 1$ ns, the diameter of such a region will be 15 cm.

The true-to-random coincidence ratio is also affected by energy selection (Muehllehner *et al* 2001). The random coincidence intensity is approximately proportional to the square of the singles-spectrum intensity. A system without septa has considerably more Compton-scattered events in the singles spectrum than in the true coincidence spectrum. Consequently, in the random coincidence spectrum there are relatively more events in the region of the Compton continuum than in the photopeak in comparison with the corresponding parts of the true coincidence spectrum. Therefore, selection of photopeak events will improve the true-to-random coincidence ratio. A good energy resolution and a high full-energy peak intensity are indeed important.

Another important aspect is dead time, i.e. the time in which a coincidence cannot be registered because the PET system is too busy handling a previous coincidence event. Several

parts of the system contribute to the dead time and the detector is one of them. Taking the BGO response time of 300 ns (scintillation decay time) as the dead time, we would lose about 3% of the events at a rate of 10^5 per second per read-out channel, which is approximately the maximum rate of a 64 scintillator–column block in a modern PET system. However, it should be noted that the actual dead time of a block is at the microsecond level due to the signal processing (shaping times). If the scintillator columns were read out individually, the rate would be only ∼1000 per second and the dead time of the scintillator/detector including electronics would be negligible.

5.2.3. Position resolution. On emission a positron travels a distance of the order of 1 mm before it is thermalized and annihilates with an electron. This electron itself has some momentum resulting in a small deviation of the angle between the annihilation quanta from 180°. These two effects contribute an additional intrinsic position resolution of up to 2 mm FWHM for a 0.8 m diameter system, dependent upon the energy, and therefore range in tissue, of the emitted positron. The intrinsic resolution decreases with decreasing system diameter.

If they are not Compton scattered in the patient, annihilation quanta emitted from the central axis of a PET system and in the plane of a detector ring will hit a scintillation detector in a direction more or less parallel to the length of the crystal columns (figure 7). Quanta emitted off-centre hit the detector at an angle. If it is not absorbed in the first crystal column encountered, the 511 keV quantum will traverse it and hit a neighbouring column well behind the detector entrance window. If it is detected there a parallax error arises. It is known as radial elongation due to its manifestation upon image reconstruction. This effect decreases with increasing system diameter, i.e. it leads to a requirement opposite to that in the previous paragraph and the large-solid-angle condition. Furthermore, for parallax reduction the length of the scintillator column should be as small as possible without loss of detection efficiency. However, for BGO a relatively long crystal, typically 30 mm, is used for efficient detection. This explains efforts to introduce methods that give depth-of-interaction (DOI) information.

A large variety of DOI methods have been studied. The response of a scintillator (light yield and decay time) is temperature dependent. This offers a possibility to extract DOI information. It was studied for NaI:Tl and BGO (Karp and Daube-Witherspoon 1987). In other studies columns of two or more different crystals in line were used for obtaining different responses as a function of depth, e.g., LSO:Ce+GSO:Ce (Saoudi *et al* 1999, Saoudi and Lecomte 1999) and LSO:Ce+GSO:Ce+BGO (Seidel *et al* 1999). In the HRRT system columns of two 7.5 mm LSO:Ce crystals with different decay times are used (Wienhard *et al* 2001). Recently, a method was presented employing avalanche photodiodes (APDs) on both sides of a 22 mm long LSO:Ce column (Shah 2001). A DOI resolution of ∼3 mm was obtained. For the many methods studied or proposed to obtain DOI information, see also Meng and Ramsden (2000).

Present PET systems have a position resolution of typically ∼4 mm FWHM in the centre of the system, increasing to ∼5–6 mm if we move in the axial direction to the edge of the system or in the radial direction to, say, 20 cm from the axis. The position resolution we are aiming at in future systems is at the level of 2–3 mm. Then the cross section of the crystal columns should be about 2×2 mm^2 and DOI information will become even more important.

As for light detection it should be mentioned that in addition to the PMTs employed in most of the PET systems described in this section, by now there are several position-sensitive light sensors available that are applicable for read out of individual scintillator columns, namely, APD arrays, position-sensitive PMTs (e.g. used in the Concorde MicroPET system)

and multi-pixel hybrid photomultipliers. The reader is referred to, e.g., Bourgeois *et al* (1999). These new sensors will certainly find their way into the field of medical imaging.

6. Inorganic scintillator development

6.1. Inorganic scintillator basics

In developing new scintillator materials, on one hand, we will in general select a material with a relatively high density ρ and high atomic number Z for efficient x-ray and gamma-ray detection (absorption probability by photoelectric effect per cm $\propto \rho Z_{\text{eff}}{}^{3-4}$). This material should transmit scintillation light efficiently and consequently we rely on ionic crystals, or crystals with some degree of covalence but with a forbidden-gap energy between valence and conduction bands, E_{gap}, large enough to transmit the emitted light. On the other hand, for good energy, time and position resolution we need a large number of scintillation photons, N_{ph}, (relative statistical spread $\propto 1/\sqrt{N_{\text{ph}}}$), and consequently the forbidden gap should be as small as possible (Rodnyi *et al* 1995):

$$N_{\text{ph}} = \frac{E}{\beta E_{\text{gap}}} SQ. \tag{1}$$

The first term on the right-hand side represents the number of thermalized electron–hole pairs $N_{\text{e–h}}$ produced by the absorption of gamma-ray energy E. The parameter β indicates the average energy required to produce one thermalized electron–hole pair: $E_{\text{e–h}} = \beta E_{\text{gap}}$, $\beta = \sim$2–3. S is the transport/transfer efficiency of the e–h pair/energy to the luminescence centre (LC) of the scintillator, and Q is the quantum efficiency of the LC, i.e. the efficiency for photon emission once the LC is excited. Of the three stages the transport/transfer, denoted by S, is the least predictable. It depends very much on defects present in the scintillator, other than the LC, that may capture electrons or holes or both, and produce radiationless transitions or afterglow upon thermal excitation. These defects can arise from the interaction itself, from crystal growing, or due to impurities; for more details see papers in Dorenbos and van Eijk (1996), Yin Zhiwen *et al* (1997) and Mikhailin (2000).

Another aspect is non-proportionality. Most scintillators have a light yield, expressed in photons per MeV of absorbed radiation energy, which is energy dependent (see e.g. Dorenbos *et al* (1995) and van Eijk *et al* (2001)). This implies that for monoenergetic gamma rays the full-energy peak resulting from photoelectric effect in a scintillator is not at the same position in the pulse height spectrum as the peak resulting from absorption of a Compton electron followed by absorption of the corresponding scattered Compton quantum. Consequently, the energy resolution is significantly degraded compared with the result expected on statistical grounds (see e.g. Valentine and Rooney (1997)). At present it is not possible to select materials for which non-proportionality effects can be estimated *a priori*.

In table 1 specifications of several scintillator materials of interest for medical imaging are summarized. Presented are the density, ρZ_{eff}^4 as a measure of the probability of interaction by photoelectric effect, the attenuation length and probability of interaction by photoelectric effect at 511 keV, hygroscopicity, light yield, decay time, for some materials afterglow information, wavelength of the emission maximum, for some scintillators energy resolution at 662 keV (FWHM) and time resolution using BaF_2 as the second, coincidence scintillator.

Of the presented materials, CsI:Na, CsI:Tl, $CdWO_4$, NaI:Tl and BGO are traditional scintillators; for reference, see van Eijk (2001) and Dorenbos *et al* (1995). Applied as an x-ray phosphor CsI:Na, CsI:Tl, $CaWO_4$, $YTaO_4$:Nb, Gd_2O_2S:Tb, Gd_2O_2S:Pr, Ce, F, Gd_2O_2S:Pr (UFC), $Y_{1.34}Gd_{0.60}O_3$:(Eu, Pr)$_{0.06}$ (Hilight) and $Gd_3Ga_5O_{12}$:Cr,Ce are partly well known. The developments will be discussed in the next section. In contrast to the scintillators just

mentioned, all of which have a relatively slow scintillation response, the Ce-based scintillators have a much faster response. The Ce^{3+} ion has one electron in the 4f state, which is lifted to the empty 5d shell upon excitation. Subsequent de-excitation will occur by an allowed $5d \rightarrow 4f$ electric dipole transition with a decay time in the order of 30 ns. These relatively new materials will also be discussed in the next section; for reference, see sections 2, 3 and 6.2.

6.2. Inorganic scintillators for medical imaging

6.2.1. X-ray scintillators. The scintillator employed most frequently in x-ray intensifying screens is Gd_2O_2S:Tb. The emission results from Tb^{3+} forbidden $4f \rightarrow 4f$ transitions. The highest intensity line is at 545 nm, i.e. in the green part of the spectrum. Examples of x-ray phosphors with blue emissions are $CaWO_4$, one of the earliest applied phosphors, and $YTaO_4$:Nb (see table 1). The emission of the former is due to the WO_4^{2-} complex that acts as a luminescence centre. Undoped $YTaO_4$ emits at ∼350 nm due to a charge-transfer transition in the tantalate group. Doping with Nb shifts the emission to a longer wavelength (see e.g. Blasse and Grabmaier (1994)).

In addition to the general detection efficiency aspects discussed in section 6.1, for x-ray detection efficiency the position of the K-edge is very important. In the energy region between the K-edges of Gd and W, which are, respectively at 50.2 and 69.5 keV, $CaWO_4$ is less sensitive to x-rays than Gd_2O_2S:Tb. $YTaO_4$:Nb is more sensitive than Gd_2O_2S:Tb at energies <50.2 keV and more sensitive than $CaWO_4$ at energies <69.5 keV. Above 69.5 keV the absorption coefficients are approximately the same. As in addition the light yields of Gd_2O_2S:Tb and $YTaO_4$:Nb are relatively high (table 1), both offer high-speed imaging using, respectively, a green- and blue-sensitive radiographic film; for more details, see e.g. Miura (1998).

Although not a scintillator, we mention $BaFBr_{1-x}I_x$:Eu ($x \leqslant 0.2$) for completeness. This storage-phosphor material was introduced in the early 1980s by Fuji (Sonoda *et al* 1983). With it the computed radiography method was presented, employing a storage-phosphor plate and photon-stimulated luminescence. In principle the operation of the storage phosphor is clear. However, the exact mechanism is still unknown. The electrons produced by x-rays are trapped in Br^- vacancies. The nature of the hole trap centres is not known (Spaeth 2001, Lakshmanan *et al* 2001). Upon optical stimulation, the trapped electron is released and electron–hole (exciton) recombination occurs under simultaneous excitation of Eu^{2+}, followed by luminescence. The addition of iodine results in a shift of both the optical stimulation spectrum and the emission spectrum to longer wavelength.

Both storage-phosphor plates and x-ray phosphor screens are formed by the addition of a binder to the phosphor powder. The ensemble is deposited on a screen base. Due to the scattering of the stimulation light at the birefringent BaFBr crystallites in a storage-phosphor plate, the position resolution is limited; for example, the resolution of ∼100 μm required for mammography could not yet be realized. In x-ray phosphor screens there is significant scintillation-light spreading by the scattering from the phosphor grains, in particular when the screen thickness is increased for x-ray detection-efficiency reasons. A method to reduce this is the application of columnar growth. This is possible with CsI:Na and CsI:Tl. Columnar screens of CsI:Na have long been mounted inside image intensifiers. The emission, due to an exciton bound to the Na^+ ion, matches well with the photocathode sensitivity. With the introduction of the a-Si:H flat-panel concept, CsI:Tl became the obvious columnar-phosphor candidate. Firstly, hygroscopic CsI:Na operates well in the vacuum of the image intensifier tube but will not do so in the flat-panel detector. CsI:Tl will not suffer from this problem as it is hardly hygroscopic in comparison with CsI:Na. Secondly, the emission spectrum of CsI:Tl,

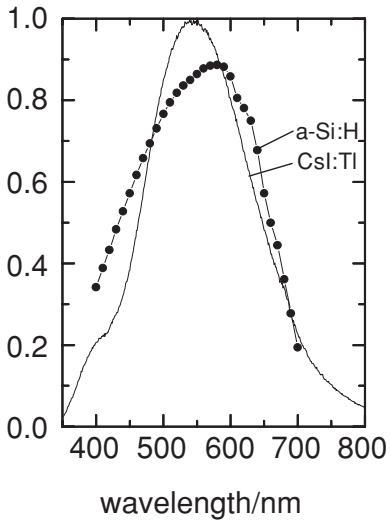

Figure 8. Matching of CsI:Tl emission spectrum with photon sensitivity of a-Si:H diodes (arbitrary units along vertical scale; courtesy Philips Research Laboratories, Aachen).

peaking at 550 nm, matches the quantum efficiency curve of amorphous silicon quite well; see figure 8.

From figure 9 an impression of the quality of columnar growth of CsI:Tl developed in recent years is obtained. The lengths of the $\sim$3 μm diameter columns are well over 0.5 mm, giving an x-ray detection efficiency at, e.g., 60 keV of $>$83%. It should be noted that the luminescence properties of these columns differ from those of CsI:Tl scintillation crystals (Garnier *et al* 2000). In addition to the two standard emission bands at 400 nm (Tl^+ emission) and 550 nm (strongly perturbed thallium-bound exciton emission), at liquid nitrogen temperature a band can be observed at 460 nm, which is attributed to a weakly perturbed thallium-bound exciton centre. At higher Tl-doping concentrations this emission disappears and the emission at 550 nm dominates. At ambient temperature the extra emission band is not observed.

As already mentioned in section 3, CsI:Tl suffers from both afterglow and an increase in light yield resulting from radiation damage (hysteresis). Recent studies resulted in a model explaining both effects by deep trapping of x-ray-generated carriers (Wieckzorec and Overdick 2000). Furthermore, the afterglow could be reduced to a level low enough for flat-panel application. Studies are being continued.

X-ray CT has flourished with the introduction of ceramic scintillators, in particular Gd_2O_2S:Pr, Ce, F, Gd_2O_2S:Pr (UFC) and $Y_{1.34}Gd_{0.60}O_3$:$(Eu, Pr)_{0.06}$, respectively, developed by Hitachi Metals (Yamada *et al* 1989), Siemens (Rossner *et al* 1999, Hupke and Doubrava 1999) (brand name UFC, ultra fast ceramics) and General Electric (Greskovich and Duclos 1997) (brand name Hilight). These polycrystalline ceramic scintillators couple good scintillation properties with homogeneity and good machinability. In addition, their emission wavelengths match well with the sensitivity of silicon diodes.

In Gd_2O_2S, or GOS, based ceramics scintillation arises from $4f \rightarrow 4f$ transitions in the Pr^{3+} dopant ion. The decay time of 3–4 μs does not pose a problem for the condition of $<$0.01% light yield after 3 ms (section 3). The afterglow is due to the trapping of charge carriers that are subsequently thermally released and recombine at luminescence centres. Co-doping with

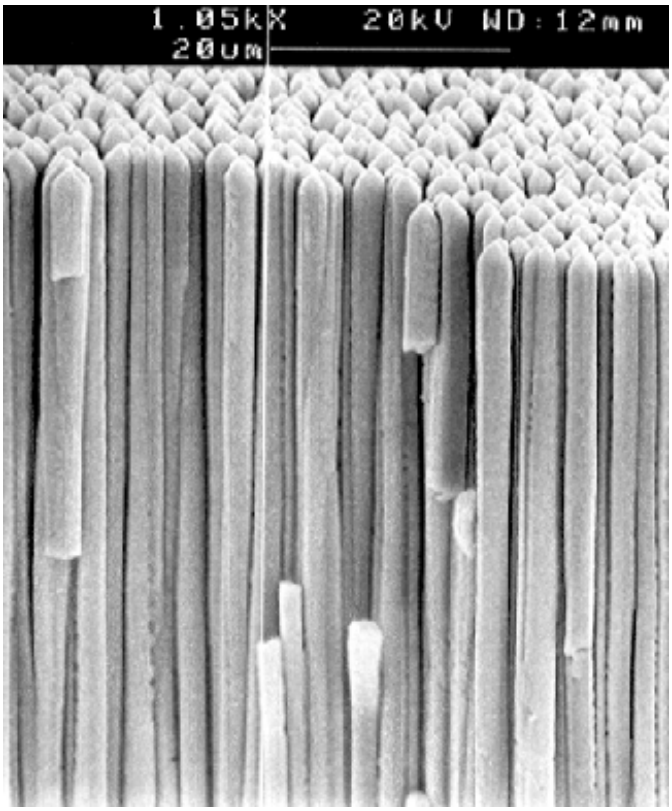

Figure 9. Vapour-deposited column-shaped CsI:Tl scintillation crystals of very smooth structure. Diameter ∼3 μm, length >0.5 mm (courtesy Philips Research Laboratories, Aachen).

cerium and fluor results in non-radiative recombination and reduction of trap centres, thus reducing the afterglow. However, the scintillation intensity is also reduced. Consequently, a compromise has to be made between light yield and afterglow reduction. It should be noted that co-doping of Gd_2O_2S:Pr with Tb and F leads to similar results (Nakamura and Ishii 2000). In UFC the afterglow reduction is primarily realized by optimized ceramic processing. From the afterglow values after 3 ms in table 1, we observe that only UFC is close to the <0.01% condition. Also, for the second condition, the light yield after 100 ms (Hupke and Doubrava 1999), UFC has the smallest value.

Due to scintillation-light scattering at the hexagonal grain boundaries in GOS-based ceramic materials these are translucent. Fortunately, relatively thin scintillation detectors can be used because of the high x-ray absorption efficiency (compare ρZ_{eff}^4 values, table 1), i.e. ∼1.5 mm compared to ∼3 mm for transparent Hilight to absorb 98% of 120 keV x-rays (Hupke and Doubrava 1999). Therefore, light collection does not pose a problem.

In $Y_{1.34}Gd_{0.60}O_3$:(Eu, Pr)$_{0.06}$, also referred to as YGO, scintillation arises from 4f → 4f transitions in the Eu^{3+} dopant ion. Pr^{3+} or Tb^{3+} co-dopant ions reduce the afterglow as they act as hole traps in competition with intrinsic traps responsible for the afterglow. The Pr or Tb sites decay non-radiatively (Greskovich and Duclos 1997). Considering the afterglow properties in table 1, we observe a much higher afterglow after 3 ms than for GOS ceramics. Hilight has the advantage of being transparent.

Another interesting ceramic scintillator is $Gd_3Ga_5O_{12}$:Cr, Ce (Greskovich and Duclos 1997). Scintillation arises from the Cr^{3+} luminescence centre and afterglow reduction from Ce^{3+} co-doping, presumably by a process similar to that in YGO. Some new ceramic materials are Lu_2O_3:Eu, Tb (Dujardin *et al* 2000, Lempicki *et al* 2001) and barium, strontium and calcium hafnates doped with cerium (Greskovich and Duclos 1997, Venkataramani *et al* 2001). In principle Lu_2O_3:Eu, Tb and the hafnates are of interest for application in both CT and PET because of their small attenuation lengths at 511 keV (table 1). However, for Lu_2O_3:Eu, Tb the decay time and afterglow are too high. Unfortunately, doping of Lu_2O_3 with cerium does not result in fast luminescence as the lowest 5d level appears to be positioned in the conduction band (Happek *et al* 2000). Of the hafnates, $SrHfO_3$:Ce has the highest light yield, ∼20 000 photons/MeV (table 1). This is somewhat small. The decay times of 25–40 ns, characteristic of Ce^{3+} emission, are very attractive. Research on these new materials is in progress.

6.2.2. Radionuclide imaging, positron emission tomography. NaI:Tl has long been the standard scintillator of the gamma camera. The luminescence is from the Tl^+ ion. The light yield is high and the emission wavelength matches the sensitivity of PMTs quite well. Crystals of large size (diameter ∼0.8 m, height ∼0.8 m) can be grown relatively easily. In principle the hygroscopicity of NaI:Tl is a disadvantage. However, canning methods are well developed.

Recently, the new scintillators $LaCl_3$:Ce and $LaBr_3$:Ce have been introduced (van Loef *et al* 2000, 2001). Their development may, among other things, be of interest for application in the gamma camera. These materials have a high light yield, fast response (Ce^{3+} ion), excellent energy resolution and very good time resolution. It should be noted that the energy and time resolution presented in table 1 have been obtained with different experimental set-ups optimized for their specific tasks (see next paragraph). The detection efficiency is comparable to that of NaI:Tl. In figure 10 we show the pulse height spectrum of the 662 keV gamma ray of ^{137}Cs recorded by means of a $LaCl_3$:Ce crystal. The energy resolution is 3.1% FWHM. The La K x-ray-escape peak can be well observed. An explanation of the small energy-resolution values of these new scintillators is most likely to be found in the very small non-proportionality (section 6.1). Both scintillators are hygroscopic to approximately the same degree as NaI:Tl. Saint-Gobain Crystals & Detectors has started the development of the new scintillators for production.

Of the scintillators in table 1 that are of interest for PET, we start the discussion with BGO (Weber and Monchamp 1973). In this material the Bi^{3+} ion is the intrinsic luminescence centre. Compared to e.g. LSO:Ce, the light yield is low and the response time long. The poor energy and time resolution obtained with BGO in a PET system (section 5) are not completely due to these less than favourable properties. Firstly it is hardly possible to efficiently collect all the scintillation light at one end of a scintillator column with a small aspect ratio. Secondly, simultaneous realization of the best energy resolution and best time resolution is a conflicting condition. Energy resolution requires a long integration time (charge integrating amplifier), for time resolution we need fast shaping. Yet, more light will lead to a significant improvement.

From the fourth column of table 1 we can deduce that a 30 mm deep BGO crystal has an interaction probability of 95% for 511 keV quanta. Of this, 38% is due to photoelectric effect and 57% due to Compton effect. Obviously in a PET system a fraction of the quanta Compton scattered in a scintillator will escape and interact in neighbouring crystals. This fraction will increase with the introduction of narrower columns for improving the position resolution (section 5). Consequently, the fraction detected in the full-energy peak will decrease and, if the energy selection window is relaxed for compensation, it will result in the opposite to what we are aiming for: deterioration of the position resolution. The Compton scattering in the

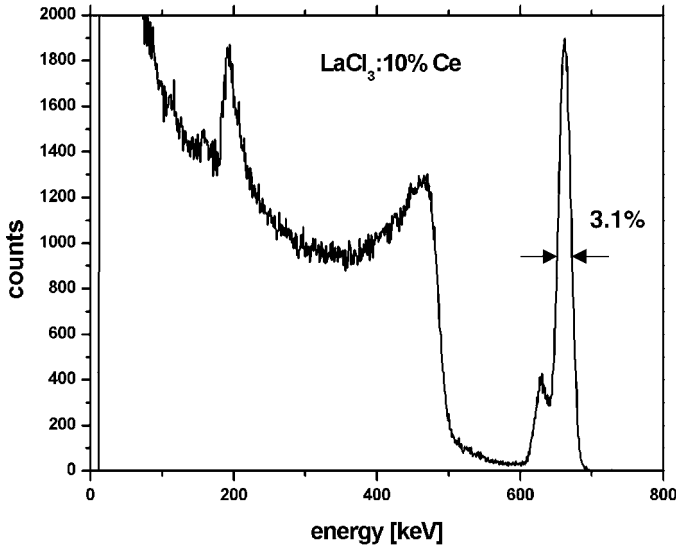

Figure 10. Pulse height spectrum of 662 keV gamma rays detected in $LaCl_3$:10%Ce crystal ($\sim 3 \times 3 \times 10$ mm^3) coupled to a PMT (R1791, shaping time 10 μs). The energy resolution of the full-energy peak is 3.1% FWHM.

forward direction has the highest probability (angle with direction of the incoming 511 keV quantum $\sim 32^\circ$). Observation of individual crystal responses and DOI will help to optimize position resolution.

LSO:Ce was introduced about 10 years ago (Melcher 1990, Melcher and Schweitzer 1992). On one hand the host material was selected for efficient detection (high ρ and Z), and on the other the Ce^{3+} LC ion can be substituted for Lu^{3+}. It appeared to be very difficult to grow large stress-free crystals ($\sim$1000 cm^3) of which small entities can be cut efficiently. These large crystals were reported to be inhomogeneous in light production and decay time, and the gamma-ray energy resolution is poorer than expected on the basis of the light yield (Melcher *et al* 1999). To some extent the latter is in agreement with the observed strong non-proportionality (Dorenbos *et al* 1995).

Using the information of column four in table 1, we deduce that 89% of the 511 keV quanta interact in the 25 mm LSO:Ce columns used in the ECAT Accel system, to be compared with 95% in 30 mm BGO. Furthermore, of the 89% an amount of 28% is due to the photoelectric effect and 61% due to the Compton effect. Obviously the process of absorption of a Compton-scattered photon in the same crystal as the Compton electron will contribute to the content of the full-energy peak. The non-proportionality, however, will result in a significantly poorer energy resolution.

Samples from different parts of a crystal boule, with different decay times, were intentionally selected for utilization in the Siemens/CTI HRRT system (section 5), thus providing DOI by pulse-shape discrimination. Note that the 511 keV interaction efficiency in 7.5 + 7.5 mm of LSO:Ce is only 73%.

Recently, the quality of LSO:Ce boules seems to have improved. LSO is available from Siemens/CTI (Knoxville, USA). Two other LSO:Ce-related scintillators are also commercially available: MLS (mixed lutetium silicate, produced by UTAR, Canada) which does not differ significantly from LSO:Ce, and $Lu_{1.8}Gd_{0.2}SiO_5$:Ce (LGSO, produced by Hitachi), which is less efficient, has a lower light yield and poorer energy resolution (Pichler *et al* 1999).

It should be noted that the application of scintillators containing lutetium has two disadvantages: (a) a high price of ∼$ 50/cm^3 due to Lu and (b) presence of the radioactive isotope ^{176}Lu which gives a count rate of ∼300 s^{-1} cm^{-3} (beta decay, end-point energy 565 keV and some gamma rays in coincidence). For PET (b) is less important.

GSO:Ce was introduced by Hitachi in the early 1980s (Takagi and Fukazawa 1983) and is still commercially available from this company. The material has a strong analogy with LSO:Ce. However, in LSO the Ce concentration is maximal at ∼0.06 mol% whereas in GSO:Ce it can easily be varied. This has an important consequence. The decay time can be varied as well. It decreases from ∼220 ns to ∼45 ns when the Ce concentration is increased from ∼0.1 mol% to ∼1 mol% (Ishibashi *et al* 1989). This phenomenon is explained by the presence of a Gd sublattice that plays an important role in transporting the available energy to the Ce ions (Dorenbos *et al* 1997). The light output is maximal at ∼0.6 mol% and consequently this is the favourable concentration, resulting in a 60 ns decay time. Originally, it was difficult to grow large crystals due to the presence of stresses, which caused cracking. However, improvements in the 1990s resulted in a technique for growing large crystals, e.g. 8 cm diameter × 28 cm length (Ishibashi *et al* 1997).

The interaction efficiency in the 20 mm long GSO:Ce crystals used in the ADAC/UGM brain PET system (section 5) is 75%. With LSO:Ce this would be 82%, with BGO 85%. Furthermore, the photopeak efficiency in GSO:Ce is smaller than that for the other scintillators and consequently it is to be expected that the content of the full-energy peak, including Compton-scattered events, is even smaller in relative measure than the total interaction numbers. The gain in energy and time resolution are clearly at the expense of efficiency.

The scintillator YAP:Ce is clearly only of interest for small-animal PET systems and we will not discuss it here in detail. The scintillator is commercially available from Saint-Gobain Crystals & Detectors and from Crytur.

LuAP:Ce is a very interesting candidate to replace BGO in PET. Its light yield is higher and the response time is much faster than those of BGO. Consequently, an excellent time resolution is expected. The energy resolution obtained so far is relatively poor. This is mainly due to the strong scintillation-light absorption, which is still an open problem. Though the probability of photoelectric effect is smaller, i.e. that of the Compton effect is higher, the attenuation length is almost identical to that of BGO. The application of LuAP:Ce in detectors with combinations of different crystals for DOI may also become interesting.

LuAP:Ce was first proposed as a scintillator in 1994 (Minkov 1994) and more detailed papers appeared shortly after (Moses *et al* 1995, Lempicki *et al* 2001). It is difficult to grow LuAP scintillation crystals. LuAP is metastable at temperatures close to the melting point. One ends up easily with $Lu_3Al_5O_{12}$(LuAG). Yet, several groups, e.g. Crytur Ltd (Turnov, Czech Republic) and A G Petrosyan (Armenian National Academy of Science), were able to supply LuAP:Ce crystals for research (Mares *et al* 1997, Dujardin *et al* 1998). Some groups tried to introduce improvements and facilitate the crystal-growing process by adding Gd or Y (Mares *et al* 1997). Light yields of 1–2 × 10^4 photons/MeV are reported for these mixed crystals, but in general longer (∼100 ns) decay time components are introduced. Research is in full progress, particularly by the Crystal Clear Collaboration at CERN.

Another relatively new scintillator with a high light yield and fast response is LPS:Ce (lutetium pyro silicate) (Pauwels *et al* 2000). The attenuation length of this scintillator is equal to that of GSO but the photopeak efficiency is higher. Consequently, LPS may be of interest for a PET system with multi-crystal detectors for DOI information. So far, only small samples of LPS have been grown. Research on this material is in progress.

From the above discussion it is clear that new scintillators have been introduced or are being developed for application in PET. It is also clear that improvements concerning energy,

time and position resolution are at the expense of efficiency. This explains why much research is going on. As already mentioned, Lu_2O_3- and $BaHfO_3$-based ceramic scintillators are, in principle, of interest for application in PET provided that better results can be realized on light yield, fast response time and energy resolution. In addition, material properties such as machinability should be favourable. Another direction, which is presently being pursued, is the upgrading of $PbWO_4$ (PWO). This scintillator was extensively studied and developed for application in high-energy physics, namely, in an electromagnetic calorimeter at CERN. The density is 8.2 g cm^{-3} and $\rho Z_{\text{eff}}^4 = 268 \times 10^6$ (see table 1 for comparison). Furthermore, the response time is fast (15 ns). However, the light yield is only 200 photons/MeV. Programmes are aiming at improving the latter by appropriate doping, without increasing the response time. So far, efforts resulted in a gain in light yield by a factor of $\sim$3. Obviously, there is a long way to go. For more information on PWO, see e.g. Mikhailin (2000).

7. Conclusions

For all medical imaging systems using x-rays or gamma rays, radiation detector development in general and scintillator development in particular are in full progress. There is a strong interest in the introduction of new dense, high-atomic-number inorganic scintillation crystals with a high light yield and a fast response, especially for PET. Ceramic scintillators are of interest for both CT and PET. For PET, research is focused on Ce^{3+} doped scintillators, employing the $5d \rightarrow 4f$ transitions. A high light yield is expected in the visible region. The time response will be in the 25–100 ns range. Improved energy resolution will also be a point of interest. For CT, time response requirements are at the microsecond level for decay time and the afterglow should be well below 10^{-4} after 3 ms. For x-ray screens light spreading should be kept under control, e.g. by columnar growth, and afterglow and hysteresis effects should be minimal.

Acknowledgments

The author is indebted to Dr V R Bom (Delft University), Dr J Jansen (Delft University), Dr C L Melcher (CTI Knoxville), G Muehllehner (ADAC/UGM Philadelphia), P F van der Stelt (Academic Center for Dentistry, Amsterdam), H Wieckzorec (Philips Research Laboratories, Aachen) and J Zoetelief (Delft University) for supplying valuable information.

References

Adam L-E, Karp J S and Daube-Witherspoon M E 2001 Evaluation of performance of the CPET scanner using standardized measurement techniques *2000 IEEE NSS/MIC Conference Record CDROM* **17** 46–50

Beyer T, Townsend D W, Brun T, Kinahan P E, Charron M, Roddy R, Jerin J, Young J, Byars L and Nutt R 2000 A combined PET/CT scanner for clinical oncology *J. Nucl. Med.* **41** 1369–79

Blasse G and Grabmaier B C 1994 *Luminescent Materials* (Berlin: Springer)

Bourgeois Ph, Fanet H, Faure J L, Goret Ph Ille B, El Mamouni H, Peigneux J P and Pouthas J (eds) 1999 Proceedings of the 2nd international conference on new developments in photon detection *Nucl. Instrum. Methods* A **442**

Casey M E and Nutt R 1986 A multicrystal two dimensional BGO detector system for positron emission tomography *IEEE Trans. Nucl. Sci.* **33** 460–63

Chepel V, Lopes M I, Kuchenkov A, Ferreira M R and Policarpo A J P L 1997 Performance study of liquid xenon detector for PET *Nucl. Instrum. Methods* A **392** 427–32

Cherry S R, Dahlbom M and Hoffman E J 1991 3D PET using a conventional multislice tomograph without septa *J. Comput. Assist. Tomogr.* **15** 655–68

Collot J, Jan S and Tournefier E 2000 A liquid xenon PET camera for neuro-science *Proc. 9th Int. Conf. on Calorimetry in High Energy Physics CALOR 2000 (Frascati Phys. Ser. 21)* ed B Aubert, J Colas, P Nédélec and L Poggioli pp 305–13

De Grado T R, Turkington T G, Williams J J, Stearns C W, Hoffman J M and Coleman R E 1994 Performance characteristics of a whole-body PET scanner *J. Nucl. Med.* **35** 1398–406

Del Guerra A, Damiani C, Di Domenico G, Motta A, Giganti M, Marchesini R, Piffanelli A, Sabba N, Sartori L and Zavattini G 2000 An integrated PET-SPECT small animal imager: preliminary results *IEEE Trans. Nucl. Sci.* **47** 1537–40

Dorenbos P, de Haas J T M and van Eijk C W E 1995 Non-proportionality in the scintillation response and the energy resolution obtainable with scintillation crystals *IEEE Trans. Nucl. Sci.* **42** 2190–202

Dorenbos P and van Eijk C W E (eds) 1996 *Proc. Int. Conf. on Inorganic Scintillators and their Applications SCINT95* (Delft: Delft University Press)

Dorenbos P, van't Spijker J C and van Eijk C W E 1997 Luminescence and scintillation mechanisms in Ce^{3+} activated Gd-compounds *Proc. Int. Conf. on Inorganic Scintillators and their Applications SCINT97* (Shanghai: Shanghai Branch Press) pp 307–10

Dujardin C, Garcia-Murillo A, Pédrini C, Madej C, Goutaudier C, Koch A, Petrosyan A G, Ovanesyan K L, Shirinyan G O and Weber M J 2000 Synthesis and scintillation properties of some dende x-ray phosphors *Proc. 5th Int. Conf. on Inorganic Scintillators and their Applications SCINT99* (Moscow: M V Lomonosov Moscow State University) pp 527–31

Dujardin C *et al* 1998 Optical and scintillation properties of large $LuAlO_3:Ce^{3+}$ *J. Phys.: Condens. Matter* **10** 3061–73

Garnier N, Dujardin C, Belsky A N C, Moy J P, Wieckzorek H, Chevallier P and Firsov A 2000 Spectroscopy of CsI(Tl) *Proc. 5th Int. Conf. on Inorganic Scintillators and their Applications SCINT99* (Moscow: M V Lomonosov Moscow State University) pp 379–84

Grabmaier B C and Rossner W 1993 New scintillators for x-ray computed tomography *Nucl. Tracks Radiat. Meas.* **21** 43–5

Gray J E, Stears J G, Swensen S J and Bunch P C 1993 Evaluation of resolution and sensitometric characteristics of an asymmetric screen-film imaging system *Radiology* **188** 537–39

Greskovich C and Duclos S 1997 Ceramic scintillators *Ann. Rev. Mater. Sci.* **27** 69–88

Happek U, Basun S A, Choi J, Krebs J K and Raukas M 2000 Electron transfer processes in rare earth doped insulators *J. Alloys Compounds* **303–304** 198–206

Hell E, Knupfer W and Mattern D 2000 The evolution of scintillating medical detectors *Nucl. Instrum. Methods* A **454** 40–8

Holl I, Lorenz E and Mageras G 1988 A measurement of the light yield of common inorganic scintillators *IEEE Trans. Nucl. Sci.* **35** 105–9

Hupke R and Doubrava C 1999 The new UFC-detector for CT-imaging *Phys. Medica* **XV** 315–8

Ishibashi H, Kurashige K, Kurata Y, Susa K, Kurosawa T, Kobayashi M, Tanaka M, Hara K and Ishii M 1997 Large Ce-doped Gd_2SiO_5 (GSO) single crystals 80 mm in diameter and its performance *Proc. Int. Conf. on Inorganic Scintillators and their Applications SCINT97* (Shanghai: Shanghai Branch Press) pp 295–98

Ishibashi H, Shimizu K, Susa K and Kubota S 1989 Cerium doped GSO scintillators and its application to position sensitive detectors *IEEE Trans. Nucl. Sci.* **36** 170–2

Jasczak R J, Coleman R E and Lim C B 1980 SPECT: single photon emission computed tomography *IEEE Trans. Nucl. Sci.* **27** 1137–53

Jing T, Goodman C A, Drewery J, Cho G, Hong W S, Lee H, Kaplan S N, Mireshghi A, Perez-Mendez V and Wildermuth D 1994 Amorphous silicon pixel layers with cesium iodide converters for medical radiography *IEEE Trans. Nucl. Sci.* **41** 903–9

Jones W F, Casey M E, van Lingen A and Bendriem B 2001 LSO PET/SPECT spatial resolution: critical on-line DOI rebinning methods and results *2000 IEEE NSS/MIC Conference Record CDROM* **16** 54–8

Kalender W A 2000 *Computed Tomography* (Munich: MCD)

Karp J S and Daube-Witherspoon M E 1987 Depth-of-interaction determination in NaI(Tl) and BGO scintillation crystals using a temperature gradient *Nucl. Instrum. Methods* A **260** 509–17

Karp J S, Surti S, Freifelder R, Daube-Witherspoon M E, Cardi C, Adam L-E, Chase B, Vaska P and Muehllehner G 2001 Performance of a GSO brain PET camera *2000 IEEE NSS/MIC Conference Record CDROM* **17** 7–11

Lakshmanan A R, Murase N, Yazawa T, Qiu J, Mitsuyu T, Hirao K, Tomoto A and Hoffmann W 2001 Luminescence studies in BaFBr and BaFBr:Eu *Radiat. Meas.* **33** 119–27

Lecoq P 2001 Clear-PEM, a dedicated PET camera for mammography *6th Int. Conf. on Inorganic Scintillators and their use in Scientific and Industrial Applications SCINT2001 (Chamonix, France 16–21 Sept. 2001)*

Lempicki A, Brecher C, Lingertat H, Szupryczynski P, Nagarkar V V, Tipnis S V and Miller S R 2001 A new scintillator for digital x-ray radiography Book of abstracts of the *6th Int. Conf. on Inorganic Scintillators and Their use in Scientific and Industrial Applications SCINT2001 (Chamonix, France, 16–21 Sept. 2001)* MI-O_02

Lempicki A, Randles M H, Wisniewski D, Balcerzyk M, Brecher C and Wojtowicz A 1995 $LuAlO_3$:Ce and other aluminate scintillators *IEEE Trans. Nucl. Sci.* **42** 280–84

Mares J A, Nikl M, Mihokova E, Kvapil J, Giba J and Blazek K 1997 Spectroscopy and transfer processes in $Lu_xGd_{1-x}AlO_3$:Ce scintillators *J. Lumin.* **72–74** 737–9

McCollough C H and Zink F E 1999 Performance evaluation of a multi-slice CT system *Med. Phys.* **26** 2223–30

Melcher C L 1990 *US Patent No* 4958080

Melcher C L, Schmand M, Eriksson M, Eriksson L, Casey M, Nutt R, Lefaucheur J L and Chai B 1999 Scintillation properties of LSO:Ce Boules *1998 IEEE Nuclear Science Symp. & Medical Imaging Conf. Record (Toronto, Ontario, Canada 8–14 Nov. 1998)* (CDROM) N9-3

Melcher C L and Schweitzer J S 1992 Cerium-doped lutetium oxyorthosilicate: a fast, efficient new scintillator *IEEE Trans. Nucl. Sci.* **39** 502–5

Meng L J and Ramsden D 2000 Performance results of a prototype depth-encoding PET detector *IEEE Trans. Nucl. Sci.* **47** 1011–17

Mikhailin V (ed) 2000 *Proc. 5th Int. Conf. on Inorganic Scintillators and their Applications SCINT99* (Moscow: M V Lomonosov Moscow State University)

Minkov B I 1994 Promising new lutetium based single crystals for fast scintillation *Functional Materials* **1** 103–05

Miura N 1998 Phosphors for x-ray and ionizing radiation *Phosphor Handbook* ed S Shionoya and W M Yen (Boca Raton, FL: CRC Press) ch 7.1 pp 521–30

Moses W W, Derenzo S E, Fyodorov A, Korzhik M, Gektin A, Minkov B and Aslanov V 1995 $LuAlO_3$:Ce—a high density, high speed scintillator for gamma detection *IEEE Trans. Nucl. Sci.* **42** 275–9

Moy J-P 1999 Recent developments in x-ray imaging detectors *Nucl. Instrum. Methods* A **442** 26–37

Muehllehner G, Karp J S and Surti S 2001 Design considerations for PET scanners *Q. J. Nucl. Med.* at press

Muller S 1999 Full-field digital mammography designed as a complete system *Eur. J. Radiol.* **31** 25–34

Nakamura R and Ishii M 2000 Improvements in the x-ray characteristics of Gd_2O_2S:Pr ceramic Scintillators *Proc. 5th Int. Conf. Inorganic Scintillators and their Applications SCINT99* 501–05 (Moscow: M V Lomonosov Moscow State University)

Neitzel U, Maack I and Günther-Hohfahl S 1994 Image quality of a digital chest radiography system based on a selenium detector *Med. Phys.* **21** 509–16

NSS/MIC 1999 Nuclear science symposium & medical imaging conference *IEEE Trans. Nucl. Sci.* **46**

NSS/MIC 2000 Nuclear science symposium & medical imaging conference *IEEE Trans. Nucl. Sci.* **47**

Pauwels D, Le Masson N, Viana B, Kahn-Harari A, van Loef E V D, Dorenbos P and van Eijk C W E 2000 A novel inorganic scintillator: $Lu_2Si_2O_7:Ce^{3+}$ (LPS) *IEEE Trans. Nucl. Sci.* **47** 1787–90

Pichler B J, Böning G, Rafecas M, Schlosshauer M, Lorenz E and Ziegler S I 1999 LGSO scintillation crystals coupled to new large area APDs compared to LSO and BGO *IEEE Trans. Nucl. Sci.* **46** 289–91

Rodnyi P A, Dorenbos P and van Eijk C W E 1995 Energy loss in inorganic scintillators *Phys. Status Solidi* b **187** 15–29

Rossner W, Ostertag M and Jermann F 1999 Properties and applications of gadolinium oxysulfide based ceramic scintillators *Electrochem. Soc. Proc.* **98-24** 187–94

Saoudi A and Lecomte R 1999 A novel APD-based detector module for multi-modality PET/SPECT/CT scanners *IEEE Trans. Nucl. Sci.* **46** 479–84

Saoudi A, Pepin C M, Dion F, Bentourkia M, Lecomte R, Andreaco M, Casey M, Nutt R and Daudet H 1999 Investigation of depth-of-interaction by pulse shape discrimination in multicrystal detectors read out by avalanche photodiodes *IEEE Trans. Nucl. Sci.* **46** 462–67

Schiebel U, Conrads N, Jung N, Weibrecht M, Wieczorek H and Zaengel T 1994 Fluoroscopic x-ray imaging with amorphous silicon thin-film arrays *SPIE Phys. Med. Imaging* **2163** 129–40

Seidel J, Vaquero J J, Siegel S, Gandler W R and Green M V 1999 Depth identification accuracy of a three layer Phoswich PET detector module *IEEE Trans. Nucl. Sci.* **46** 485–90

Shah K S, Farrell R, Grazioso R, Shao Y and Cherry S R 2001 APD arrays for medical imaging, *6th Int. Conf. on Inorganic Scintillators and their use in Scientific and Industrial Applications SCINT2001 (Chamonix, France, 16–21 Sept. 2001)*

Short M D 1984 Gamma camera systems *Nucl. Instrum. Methods* **221** 142–9

Soltani P K, Wysnewski D and Swartz K 1999 Amorphous selenium direct radiography for industrial imaging *Proc. Computerized Tomography and Image Processing* (Berlin: DGZfP Proceedings BB 67-CD) pp 123–32

Sonoda M, Takano M, Miyahara J and Kato H 1983 Computed radiography utilizing scanning laser stimulated luminescence *Radiology* **148** 833–8

Spaeth J-M 2001 Recent developments in x-ray storage phosphor materials *Radiat. Meas.* **33** 527–32

Takagi K and Fukazawa T 1983 Cerium-activated Gd_2SiO_5 single crystal scintillator *Appl. Phys. Lett.* **42** 43–5

Townsend D W 2001 New trends in PET scanners presented by C Morel at the *6th Int. Conf. on Inorganic Scintillators and their use in Scientific and Industrial Applications SCINT2001 (Chamonix, France, 16–21 Sept. 2001)*

Townsend D W, Spinks T J, Jones T, Geissbühler A, Defrise M, Gilardi M C and Heather J 1989 Three-dimensional reconstruction of PET data from a multi-ring camera *IEEE Trans. Nucl. Sci.* **36** 1056–65

Valentine J D and Rooney B D 1997 Intrinsic energy resolution and its dependence on light yield nonproportionality *Proc. Int. Conf. on Inorganic Scintillators and their Applications SCINT97* (Shanghai: Shanghai Branch Press) pp 91–4

van der Stelt P F 2001 The implementation of digital sensors in maxillofacial radiography *Nucl. Instrum. Methods* A **460** 45–9

van Eijk C W E 2001 Inorganic-scintillator development *Nucl. Instrum. Methods* A **460** 1–4

van Eijk C W E, Dorenbos P, van Loef E V D, Krämer K and Güdel H U 2001 Energy resolution of some new inorganic-scintillator gamma-ray detectors *Radiat. Meas.* **33** 521–5

van Loef E V D, Dorenbos P, van Eijk C W E, Krämer K and Güdel H U 2000 High-energy-resolution scintillator: Ce^{3+} activated $LaCl_3$ *Appl. Phys. Lett.* **77** 1467–8

van Loef E V D, Dorenbos P, van Eijk C W E, Krämer K and Güdel H U 2001 High-energy-resolution scintillator: Ce^{3+} activated $LaBr_3$ *Appl. Phys. Lett.* **79** 1573–5

Venkataramani V, Loureiro S, Rane M, Duclos S, Stearns C and McDaniel D 2001 Transparant ceramic routes to scintillators *2001 IEEE Nuclear Science Symp & Medical Imaging Conf. (San Diego, CA, N8–4, 4–10 Nov. 2001)* at press

Webb S (ed) 1990 *The Physics of Medical Imaging* (Bristol: Adam Hilger)

Weber S, Bauer A, Herzog H, Kehren F, Mühlensiepen H, Vogelbruch J, Coenen H H, Zilles K and Halling H 2000 Recent results of the TierPET Scanner *IEEE Trans. Nucl. Sci.* **47** 1665–9

Weber M J and Monchamp R R 1973 Luminescence of $Bi_4Ge_3O_{12}$: spectral and decay properties *J. Appl. Phys.* **44** 5495–9

Wieckzorec H and Overdick M 2000 Afterglow and hysteresis in CsI:Tl *Proc. 5th Int. Conf. on Inorganic Scintillators and their Applications* (Moscow: M L Lomonosov Moscow State University) pp 385–90

Wienhard K, Dahlbom M, Eriksson L, Michel C, Bruckbauer T, Pietrzyk U and Heiss W-D 1994 The ECAT EXACT HR: performance of a new high resolution positron scanner *J. Comput. Assist. Tomogr.* **18** 110–8

Wienhard K *et al* 2001 The ECAT HRRT: performance and first clinical application of the new high resolution research tomograph *2000 IEEE NSS/MIC Conference Record CDROM* **17** 2–6

Williams J R and Thwaites D I 2000 *Radiotherapy Physics in Practice* (Oxford: Oxford University Press)

Yamada H, Suzuki A, Uchida Y, Yoschida M and Yamamoto H 1989 A scintillator Gd_2O_2S:Pr,Ce,F for x-ray computed tomography *J. Electrochem. Soc.* **136** 2713–20

Yin Zhiwen, Feng Xiqi, Li Peijun and Xue Zhilin (eds) 1997 *Proc. Int. Conf. on Inorganic Scintillators and their Applications SCINT97* (Shanghai: Shanghai Institute of Ceramics, Chinese Academy of Sciences, Shanghai Branch Press)